ELSEVIER

NeuroImage

www.elsevier.com/locate/ynimg
NeuroImage 40 (2008) 570–582

# Stereotaxic white matter atlas based on diffusion tensor imaging in an ICBM template

Susumu Mori,[a,b,*] Kenichi Oishi,[a] Hangyi Jiang,[a,b] Li Jiang,[b] Xin Li,[b] Kazi Akhter,[a] Kegang Hua,[a,b] Andreia V. Faria,[a] Asif Mahmood,[b] Roger Woods,[d] Arthur W. Toga,[e] G. Bruce Pike,[f] Pedro Rosa Neto,[f] Alan Evans,[f] Jiangyang Zhang,[a] Hao Huang,[a] Michael I. Miller,[c] Peter van Zijl,[a,b] and John Mazziotta[d]

[a]*The Russell H. Morgan Department of Radiology and Radiological Science, The Johns Hopkins University School of Medicine, Baltimore, MD, USA*
[b]*F.M. Kirby Research Center for Functional Brain Imaging, Kennedy Krieger Institute, Baltimore, MD, USA*
[c]*Department of Biomedical Engineering, The Johns Hopkins University School of Medicine, Baltimore, MD, USA*
[d]*UCLA Brain Mapping Center, Department of Neurology and Radiology, University of California Los Angeles, School of Medicine, Los Angeles, CA, USA*
[f]*Laboratory of Neuro Imaging, Department of Neurology, University of California Los Angeles, School of Medicine, Los Angeles, CA, USA*
[e]*McConnell Brain Imaging Centre, Montreal Neurological Institute, McGill University, Montreal, Canada*

Received 23 July 2007; revised 6 November 2007; accepted 14 December 2007
Available online 3 January 2008

**Brain registration to a stereotaxic atlas is an effective way to report anatomic locations of interest and to perform anatomic quantification. However, existing stereotaxic atlases lack comprehensive coordinate information about white matter structures. In this paper, white matter-specific atlases in stereotaxic coordinates are introduced. As a reference template, the widely used ICBM-152 was used. The atlas contains fiber orientation maps and hand-segmented white matter parcellation maps based on diffusion tensor imaging (DTI). Registration accuracy by linear and non-linear transformation was measured, and automated template-based white matter parcellation was tested. The results showed a high correlation between the manual ROI-based and the automated approaches for normal adult populations. The atlases are freely available and believed to be a useful resource as a target template and for automated parcellation methods.**


## Introduction

Stereotaxic human brain atlases play an important role in brain research. One of the most widely used atlases is one by Talairach and Tournoux (1988), which is based on histology data from a single subject. The atlas contains a cytoarchitectural map of the cortex through the addition of Brodmann's (1909) map, explaining its wide use for registering, identifying, and reporting human cortical locations in a common coordinate system (Lancaster et al., 2000). A series of probabilistic maps provided by the Montreal Neurological Institute (MNI) and the International Consortium of Brain Mapping (ICBM) are also widely used (Collins et al., 1994; Evans et al., 1992; Mazziotta et al., 1995). These maps were created by linearly registering a large number of T1-weighted MR images of normal subjects into a common template. These maps have excellent values as a target template for normalization-based group analyses. However, in these existing atlases, the amount of information about white matter anatomy is limited (Toga et al., 2006). This lack of white matter information is understandable because this tissue appears homogeneous in conventional MRI, as well as in histology preparations. Such a lack of anatomical clues, contrary to gyral and sulcal patterns in the cortex, renders identification and delineation of specific white matter locations very difficult.

Diffusion tensor imaging is a relatively new MR modality (Basser et al., 1994a), with which we can visualize various axonal bundles within the white matter, based on orientational information (Catani et al., 2002; Douek et al., 1991; Jellison et al., 2004; Makris et al., 1997; Mori et al., 2002; Nakada and Matsuzawa, 1995; Pajevic and Pierpaoli, 1999; Pierpaoli et al., 1996; Stieltjes et al., 2001). This orientation-based contrast opens up new opportunities to establish a white matter coordinate system and study disease mechanisms or relationship between anatomy and functions of white matter. To understand disease patterns (e.g., the lesion frequency in a specific white matter location) or to correlate these anatomic abnormalities with functional deficits using group statistical analyses, lesion lo-

* Corresponding author. The Russell H. Morgan Department of Radiology and Radiological Science, The Johns Hopkins University School of Medicine, 217 Traylor Building, 720 Rutland Ave, Baltimore, MD 21205, USA. Fax: +1 410 614 1978.
*E-mail address:* susumu@mri.jhu.edu (S. Mori).
**Available online on ScienceDirect (www.sciencedirect.com).**

1053-8119/$ - see front matter © 2008 Elsevier Inc. All rights reserved.
doi:10.1016/j.neuroimage.2007.12.035

cations must be described by a coordinate system. DTI information can be used to generate "addresses" based on anatomic units in otherwise homogeneous-looking white matter, which is the first step toward the establishment of a white matter functional map similar to cortical functional maps. Establishing a standard coordinate system for white matter and developing tools to utilize it are thus of great importance. In this paper, we introduce a stereotaxic population-averaged white matter atlas, in which we fused DTI-based white matter information with an existing anatomical template (ICBM-152). This atlas is based on tensor maps obtained from 81 normal subjects acquired under an initiative of the International Consortium of Brain Mapping (ICBM). A hand-segmented white matter parcellation map was created from this averaged map, which can be used for automated white matter parcellation. The precision of the affine-based image normalization and automated parcellation was measured for a group of normal subjects using manually defined anatomical landmarks.

## Methods and materials

### *Creation of the population-averaged atlas in the ICBM-152 coordinates (ICBM-DTI-81)*

DTI data obtained from 81 normal subjects were used for the population-averaged atlas. The data were acquired at the Montreal Neurological Institute (24 cases) and University of California Los Angeles (57 cases) under the International Consortium of Brain Mapping (ICBM) collaboration (M: 42, F: 39, average age: 38. 63 (18–59 years old), right-handed). All studies were obtained on 1.5 T MR units (Siemens, Sonata, VA25 operating system). DT imaging data were acquired by using a single-shot, echo-planar imaging sequence with sensitivity encoding and a parallel imaging factor of 2.0 (Pruessmann et al., 1999). The imaging matrix was 96×96 with a field of view of 240×240 mm (nominal resolution: 2.5 mm). Transverse sections of 2.5 mm thickness were acquired parallel to the anterior commissure–posterior commissure line (AC–PC). A total of 60 sections covered the entire hemisphere and brainstem without gaps. Diffusion weighting was encoded along 30 independent orientations (Jones et al., 1999) and the *b*-value was 1000 s/mm$^2$.

Five additional images with minimal diffusion weighting were also acquired. The scanning time per dataset was approximately 4 min. To enhance the signal-to-noise ratio, imaging was repeated three times.

To remove mis-registration due to subject motion- and eddy-current-induced image distortion, the raw diffusion-weighted images (DWIs) were co-registered to one of the least diffusion-weighted images using 12-mode affine transformation with Automated Image Registration (AIR) (Woods et al., 1998). The average of all DWIs (aDWI) was calculated and used for a DTI-based anatomic image. The six elements of the diffusion tensor were calculated for each pixel with multivariate linear fitting using DtiStudio (H. Jiang and S. Mori, Johns Hopkins University, Kennedy Krieger Institute) (Basser et al., 1994b; Jiang et al., 2006). After diagonalization, three eigenvalues and eigenvectors were obtained. For the anisotropy map, fractional anisotropy (FA) was used (Pierpaoli and Basser, 1996). The eigenvector (v1) associated with the largest eigenvalue was used as an indicator for fiber orientation. A 24-bit color-coded orientation map was created by assigning red, green, and blue channels to the *x* (right–left), *y* (anterior–posterior), and *z* (superior–inferior) components of the v1 and its intensity was modulated by FA.

For anatomical images to drive the normalization process, aDWIs were used. These images were normalized to the template (ICBM-152) using a 12-mode affine transformation of AIR. The transformation matrix was then applied to the calculated diffusion tensor field, based on the method described by Alexander et al. (2001) and Xu et al. (2003). The entire normalization process was performed by in-house software called Landmarker (X. Li, H. Jiang, and S. Mori, Johns Hopkins University, www.MriStudio.org or mri.kennedykrieger.org) and took approximately 30 min for the entire process. After normalization, the image matrix and pixel resolution were interpolated to match those of the ICBM-152 (181×217×181 with 1 mm pixel resolution) using trilinear interpolation. To obtain population-averaged data, the linearly transformed tensor fields from individual subjects were averaged by simple scalar averaging of tensor elements. From the averaged tensor field, the FA and color-coded maps were recalculated. An additional nine normal subjects, who were not included in the atlas-making, were also normalized using an affine or fourth-order polynomial non-linear transformation by AIR to test the accuracy of atlas registration. For all AIR-based normalization, the ratio image uniformity (RIU) cost function was used (Woods et al., 1998).

### *White matter parcellation map (WMPM)*

Based on fiber orientation information visualized in the color-coded map, the white matter was segmented, and will be referred to as the White Matter Pacellation Map (WMPM) hereafter. In the WMPM, deep white matter regions were manually segmented into various anatomic regions. The partition criteria were derived from histology-based atlases (Carpenter, 1976; Crosby et al., 1962; Nieuwenhuys et al., 1983).

Definition of structures in the white matter is sometimes confusing. For example, names, such as the internal capsule, refer to specific locations in the white matter. This structure contains various axonal tracts with different trajectories (i.e., corticospinal tract, corticopontine tract, corticothalamic tract, thalamocortical tract, etc.). On the other hand, nomenclature such as the corticospinal and corticopontine refers to the connection between two anatomic regions, although the separation of these two types of nomenclature is not always clear in white matter anatomy.

The WMPM is primarily based on the former nomenclature. The connection-based assignment of white matter structures has been made possible by tractography-based methods (Basser et al., 2000; Conturo et al., 1999; Mori et al., 1999; Parker et al., 2002; Poupon et al., 2000; Wakana et al., 2004). However, these methods have several limitations: (1) only a limited region of white matter can be assigned by tractography with known validity; and (2) occasionally, the same regions are labeled by multiple tracking results. Because of these limitations, the white matter parcellation is primarily based on hand segmentation while tractography-based tract identification is provided as a secondary source of white matter parcellation.

As described below, the definition of the parcellation boundaries is sometimes arbitrary. This is inevitable because tissue anatomy often does not have clear boundaries. This is, again, similar to city boundaries on a map. Sometimes, there is a clear boundary, such as a river, but sometimes, the definition is artificial. The resultant map could be nonetheless useful for establishing coordinates. In the following description of each WMPM partition, such artificial boundaries, when used, are explicitly described. For detailed pictorial

views of the nomenclature and locations of the white matter structures, please refer to our previous white matter atlases (Mori et al., 2005; Wakana et al., 2004).

In the WMPM, the following white matter structures are identified and partitioned:

(1) *Tracts in the brainstem*

*Corticospinal tracts (CST):* This structure can be clearly identified at the medulla and the pons level, but should also contain corticopontine and corticobulbar tracts.

*Medial lemniscus (ML):* This is a major sensory pathway toward the thalamus. This tract is identifiable in the pons, but not in the midbrain. Because of the limited image resolution, this parcellation may include the central tegmental tract.

*Medial longitudinal fasciculus (MLF):* This fiber bundle, running along the medial dorsal aspect of the brainstem, connects various nuclei in the brainstem.

*Inferior cerebellar peduncle (ICP):* This tract carries information from the spinal cord and the medulla to the cerebellum.

*Middle cerebellar peduncle (MCP):* This massive tract initiates from the pontine nuclei and carries information between the cortex and the cerebellum. In the pons, this segment also contains pontine crossing fibers. This tract continues to the cerebellar white matter and its boundary is not clear. In our map, the white matter ventral to the dentate nuclei is defined as the MCP.

*Superior cerebellar peduncle (SCP):* This tract carries information between the deep cerebellar nuclei (dentate nuclei) and the thalamus. This tract is identifiable from the cerebellar nuclei to the midbrain at the SCP deccusation. After the deccusation, the tract cannot be identified with current image resolution.

(2) *Projection fibers*

Corona radiata: This structure is divided into three regions: anterior (ACR), superior (SCR), and posterior (PCR). The divisions are made at the middle of the genu and splenium of the corpus callosum, which are arbitrarily chosen and not based on anatomic or functional boundaries. This region includes the thalamic radiations (thalamocortical, corticothalamic fibers) and parts of the long corticofugal pathways, such as the corticospinal, corticopontine, and corticobulbar tracts. The boundary of the corona radiata and the internal capsule is defined at the axial level where the internal capsule and the external capsule merge.

*Anterior limb of internal capsule (ALIC):* The anterior thalamic radiation and fronto-pontine fibers are the major contributors in this region.

*Posterior limb of internal capsule (PLIC):* The superior thalamic radiation and long corticofugal pathways, such as the corticospinal tract and the fronto- and parieto-pontine fibers, are the major constituents.

*Retrolenticular part of the internal capsule (RLIC):* In this region, the posterior thalamic radiation (corticothalamic and thalamocortical fibers, including the optic radiation) is the major constituent, but can also include the parieto-, occipito- and temporopontine fibers. The boundary with the sagittal stratum (SS) is arbitrarily defined at the middle of the splenium of the corpus callosum.

*Cerebral peduncle (CP):* This is a region where long corticofugal pathways are concentrated, including the corticospinal, corticopontine, and corticobulbar tracts. The boundary between the cerebral peduncle and the internal capsule is defined at the axial level below the anterior commissure.

(3) *Association fibers*

*Superior longitudinal fasciculus (SLF):* This tract is located at the dorsolateral regions of the corona radiata and contains connections between the frontal, parietal, occipital, and temporal lobes including language-related areas (Broca's, Geschwind's, and Wernicke's territories).

*Superior fronto-occipital fasciculus (SFO):* This tract is located at the superior edge of the anterior limb of the internal capsule (anterior thalamic radiation) and the boundary is not always clear. Only the frontal region is identifiable and projection to the parietal lobe cannot be segmented. It has been suggested that this tract is a part of the anterior thalamic radiation and not an association fiber (Ture et al., 1997).

*Uncinate fasciculus (UNC):* This tract connects the frontal lobe (orbital cortex) and the anterior temporal lobe. It can be discretely identified where the two lobes are connected but not within the frontal and the temporal lobes where it merges with other tracts.

*Inferior fronto-occipital fasciculus (IFO)/Uncinate fasciculus (UNC):* The IFO connects the frontal lobe and the occipital lobe. In the frontal lobe, this partition also includes the frontal projection of the UNC. In the temporal and occipital lobe, the IFO merges with the inferior longitudinal fasciculus (ILF), which is segmented as a different partition.

*Inferior fronto-occipital fasciculus (IFO)/Inferior longitudinal fasciculus (ILF):* This partition includes the white matter in the temporal and occipital lobe where the IFO and the ILF are the major constituents. The ILF connects the temporal lobe and the occipital lobes. It cannot be distinguished from the IFO in most of the temporal and occipital white matter.

*Sagittal stratum (SS):* The IFO/ILF merges with projection fibers from the RLIC and forms a large, sheet-like, sagittal structure, called the sagittal stratum. This region, therefore, should include both association and projection fibers. The boundary of the IFO/ILF and SS is arbitrarily defined at the axial level of the anterior commissure. The boundary of the SS and the PCR is also arbitrarily defined at the axial level of the splenium of the corpus callosum.

*External capsule (EC):* This region, located lateral to the internal capsule, is believed to contain association fibers, such as the SLF and IFO and commissural fibers. Because of the limited image resolution, the external and extreme capsules are not resolved.

*Cingulum (CG):* This tract carries information from the cingulate gyrus to the hippocampus. The entire pathway from the frontal lobe to the temporal lobe can be clearly identified. In the WMPM, the CG in the cingulate gyrus and the hippocampal regions is separated at the axial level of the splenium of the corpus callosum and denoted as CgC and CgH, respectively.

*Fornix (FX) and stria terminalis (ST):* These tracts are both related to the limbic system: the FX to the hippocampus, and the ST to the amygdala. Both tracts project to the septum and the hypothalamus. With current image resolution capabilities, these two tracts cannot be distinguished in the hippocampal area, and both tracts are labeled as FX. The ST can be discretely identified in the amygdala and the dorsal thalamus.

(4) *Commissural fibers*

*Anterior commissure (AC):* The projection to the temporal lobes of the AC is segmented.

*Corpus callosum (CC):* This partition contains the corpus callosum and the boundary extends until it merges with the corona radiata. The CC is further divided into the genu (GCC), the body (BCC), and the splenium (SCC) regions with arbitrary boundaries.

*Tapetum (TAP):* This temporal component of the CC is partitioned separately from the other CC regions.

The current WMPM does not include the partition of subcortical white matter because of difficulties in assigning and defining boundaries in these regions. Their assignment could be an important future effort, using techniques such as those suggested by Makris et al. (Makris et al., 2005).

*Measurement of registration quality*

Data from 9 normal subjects, which were not included in the atlas making, were used for the measurements of registration quality. In these measurements, 237 anatomical landmarks were manually placed on white matter structures that were readily identifiable: 15 in the mid-sagittal plane; 158 in eight axial planes; and 64 in five coronal planes (see Appendix for the MNI coordinates of the 237 landmarks). For the landmark placement MriStudio/Landmarker was used. These landmarks were first placed in the atlases, which are called the "standard landmark set." The 9 normal subject brains were then normalized to these atlases using an affine transformation. The standard landmarks were then copied onto the normalized subject data and moved to the corresponding anatomical locations. The distance of the landmark displacement was measured ($\bar{d}$), which represented the residual anatomical difference between the subjects and the atlases. For image normalization of these test data, affine and fourth-order non-linear transformations were used. The measurement results, $\bar{d}$, from these two methods were compared using Mann–Whiney test.

*Evaluation of the atlas-guided manual and automated quantification of FA values*

We tested manual and automated measurements of pixel intensities using the WMPM. Fig. 1 summarizes the four different approaches tested. In all approaches, we first determined the anatomical regions to measure using the ICBM-DTI-81 atlas, as shown in Figs. 1B and C (13 regions in an axial [$z=79$] slice and 13 regions in a coronal slice [$y=104$]). The WMPM in these slices served as a guide for the shapes and sizes of regions of interest (ROIs). For the "manual" approach, the slices corresponding to the atlas, [$z=79$] and [$y=104$], were chosen by subjective judgment in each subject, and the 26 anatomical regions defined in the WMPM

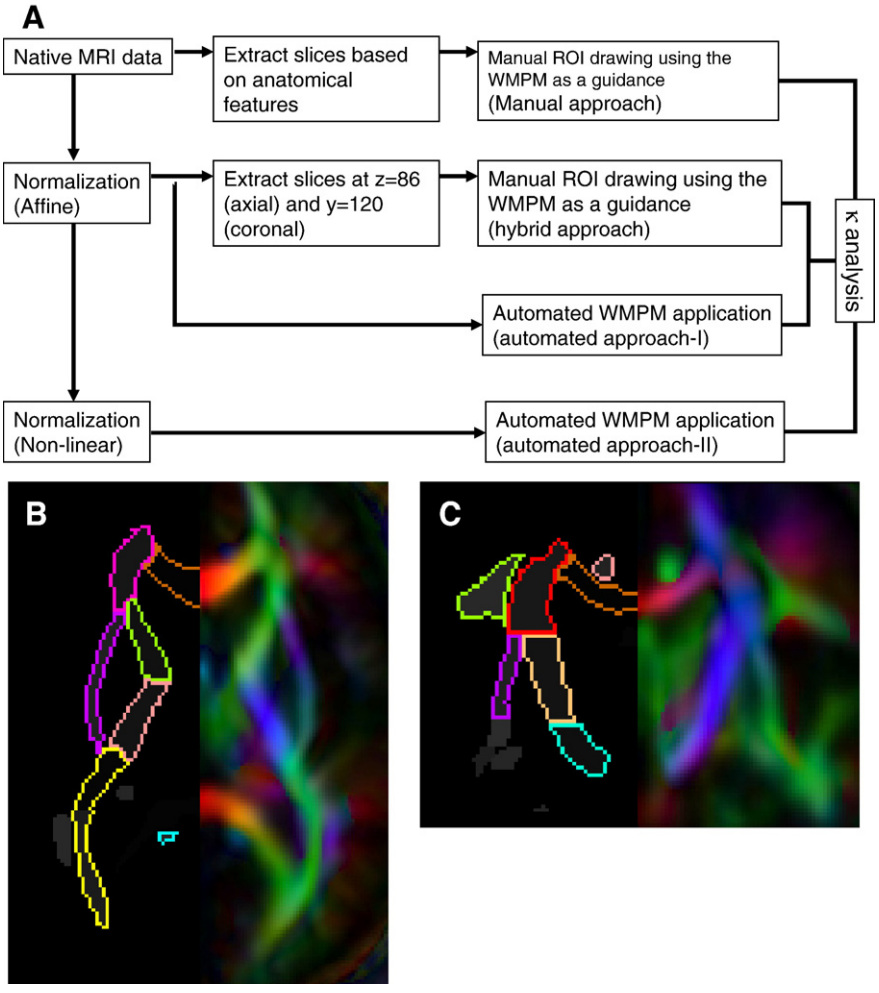


Fig. 1. (A) Procedures for WMPM-based ROI-drawing and automated methods for pixel intensity (FA) measurements. In this study, four different approaches are compared: manual; hybrid; Automated I; and Automated II. (B and C) 26 anatomical regions [13 in an axial (B) and 13 in a coronal (C) slice] defined by the WMPM and used for the FA measurements in this study. Except for the ROI for the corpus callosum, the ROIs were placed in both hemispheres. For the manual and hybrid approaches, ROIs are manually delineated using the WMPM as a guide. For Automated I and II, the WMPM is applied automatically after brain normalization.

were delineated manually. This hybrid approach is similar to the "manual" approach except that the subject data were first normalized to the ICBM-152 template and the observation planes were extracted at $z=79$ (axial) and $y=104$ (coronal), thus eliminating the step of subjectively identifying the planes. These approaches were applied to 10 normal subjects. Using two of the subjects, the measurements were repeated three times by the same rater (intra-rater variability) and by three raters (inter-rater variability). For the automated approach, the WMPM was automatically applied to the normalized images, and FA values of the 26 regions were measured. Both the manual and automated approaches were performed by our in-house software, MriStudio/RoiEditor (www.MriStudio.org or mri.kennedykrieger.org). For the intra- and inter-rater reproducibility, the degree of spatial matching was also measured using $\kappa$ analysis.

## Results

Fig. 2 shows the ICBM-152 used as the template in this study (Fig. 2A), and co-registered DTI-derived maps (Figs. 2B–D). The ICBM-152 template is based on T1-weighted images of 152 normal volunteers. While this template is widely used for anatomical and functional MRI studies, it does not provide detailed information about white matter anatomy. The DTI-based atlas created in this study complements this template by providing information about the white matter anatomy in the same standardized coordinates. Figs. 2E–H show several slices of the color-coded orientation maps in the ICBM-DTI-81 atlas. The stems of many major white matter tracts can be readily appreciated. Those tracts appreciable in the ICBM-DTI-81 atlas indicate that their existence and locations are reproducible among normal subjects. For example, the stem of the uncinate fasciculus (red arrow), the cingulum (yellow), a branch of the superior longitudinal fasciculus (orange), and the subcortical white matter of the superior temporal gyrus (white) can be clearly identified.

The WMPM was created based on these stable structures identified in the ICBM-DTI-81 atlas. The map was superimposed on the ICBM-152 and the ICBM-DTI-81 and is shown in Fig. 3. Almost perfect superimposition of the WMPM and ICBM-512 indicates the WMPM's applicability to the widely used ICBM-152 space.

The quality of white matter normalization by linear and non-linear transformation was measured by manually placed landmarks. In Fig. 4A, the cumulative distributions of landmark displacement after linear and non-linear transformation are shown. It can be seen that 90% (linear) or 95% (non-linear) of the landmarks placed in individuals are within approximately 3 mm of corresponding white matter structures in the ICBM-DTI-81 atlas. Mann–Whitney test indicates significant improvement by non-linear transformation ($P<\alpha$, $\alpha=0.005$). The displacement map was also calculated from the amount of displacement (average of the nine subjects) at each landmark location. The map (Fig. 4B) shows that the distribution of the mismatch is mostly homogeneous throughout the brain. This map can be used to estimate the accuracy of normalization at any given brain region or segment of interest.

We tested template-based manual and automated white matter parcellation and FA measurements using the WMPM in (Fig. 1). In Table 1, reproducibility measurement results of the "manual" and "hybrid" methods are tabulated. These results were calculated from the measurements performed on the 26 anatomical regions, repeated three times (intra-rater) or by four raters (inter-rater) using representative data from two subjects. In both approaches, the WMPM was used as guide for ROI drawing. In the manual approach, visual selection of the axial slice and manual ROI drawing affect the reproducibility, while, in the hybrid approach, only the latter contributes to reproducibility. Both

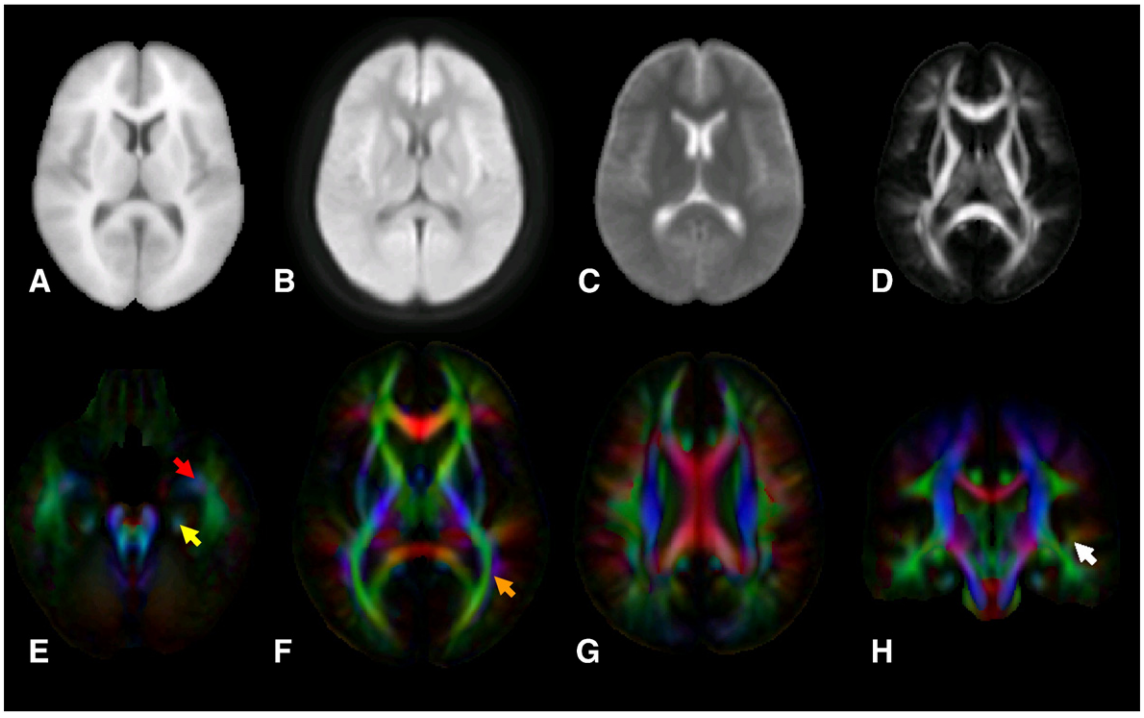


Fig. 2. Various contrasts obtained from the ICBM-DTI-81 atlas. (A–D) An axial slice from ICBM-152 (A) and aDWI (B), minimally diffusion-weighted (C), and FA maps (D) from ICBM-DTI-81. (E–H) Color-coded orientation maps from ICBM-DTI-81 at four different axial slices.

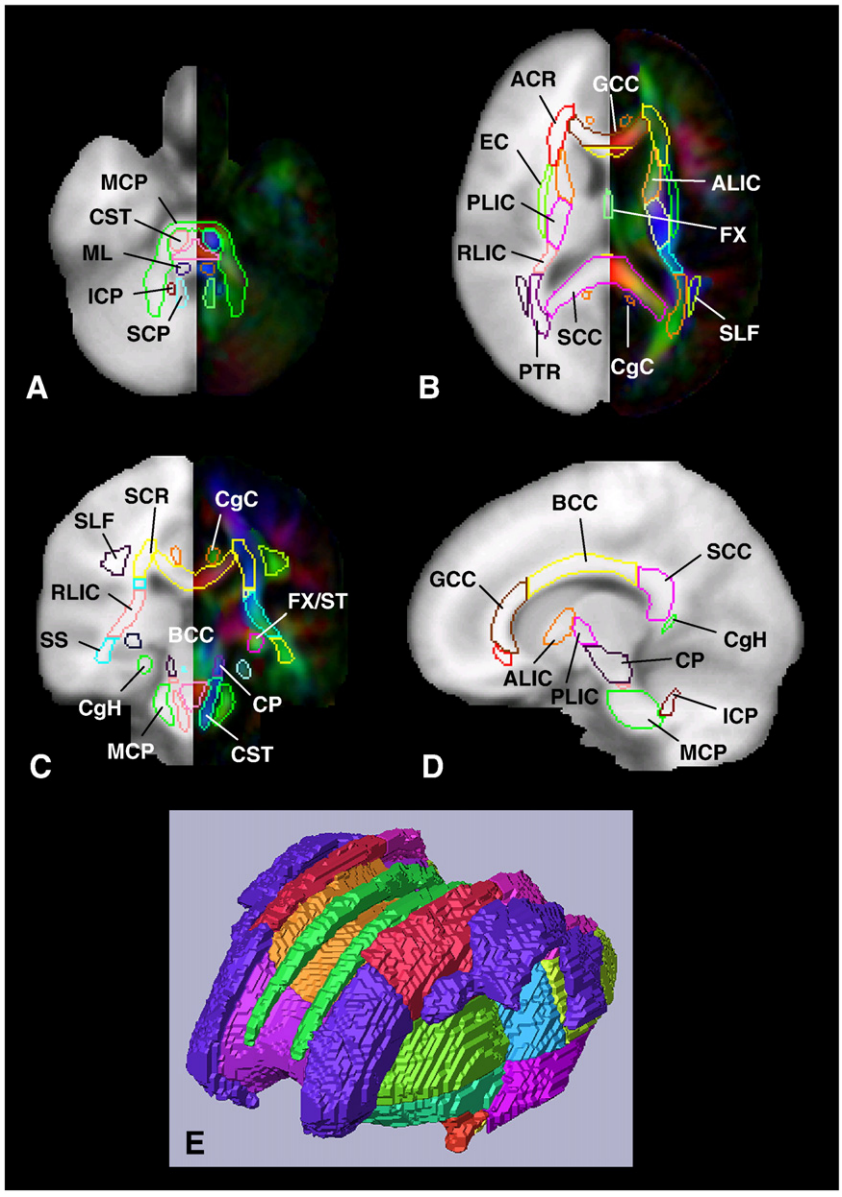


Fig. 3. Two-dimensional (A–D) and three-dimensional (E) presentation of the WMPM. For the two-dimensional view, the WMPM is superimposed on the ICBM-152 (left) and ICBM-DTI-81 (right). The abbreviations are: ACR: anterior corona radiata; ALIC: anterior limb of the internal capsule; BCC: body of the corpus callosum; CgC: cingulum in the cingulate cortex; CgH: cingulum in the hippocampus; CP: cerebral peduncle; CST: corticospinal tract; EC: external capsule; FX: fornix; GCC: genu of the corpus callosum; ICP: inferior cerebellar peduncle; MCP: middle cerebellar peduncle; ML: medial lemniscus; PLIC: posterior limb of the internal capsule; RLIC: retrolenticular part of the internal capsule; PTR: posterior thalamic radiation; SCC: splenium of the corpus callosum; SCP: superior cerebellar peduncle; SCR: superior corona radiata; SLF: superior longitudinal fasciculus; SS: sagittal stratum.

approaches have a high degree of spatial matching ($\kappa$) for intra-rater reproducibility ($\kappa > 0.86$, considered almost perfect matching), indicating that the WMPM is an effective guide for ROI drawing. The inter-rater reproducibility using the hybrid approach also shows high reproducibility ($\kappa = 0.781$), while that of the manual approach is poor because, on some occasions, different axial slices were selected by different raters, leading to $\kappa = 0$. This reproducibility issue in slice selection is effectively removed by the hybrid approach. The coefficient of variation for the intra-rater and inter-rater measurements are less than 3% except for the inter-rater value of the manual approach. Please note that the reproducibility measurements are not necessary for automated methods because perfect reproducibility ($\kappa = 1$) is expected.

The four different methods were applied to DTI data from 10 normal subjects, and FAs at the 13 anatomical regions were measured for the representative axial and the coronal slices. In Fig. 5, correlation results between the four different methods are shown, in which the hybrid results are used as a reference. Correlations of these methods are all high ($R^2 > 0.94$), indicating that all approaches could differentiate the characteristic FA value of each anatomical region. However, the automated method using the linear transformation has noticeably higher standard deviation among the normal population. Coefficients of variation among the normal population are 9.3 ± 4.1%, 10.0 ± 5.3%, 14.2 ± 12.1%, and 10.9 ± 7.1% for the manual, hybrid, automated-I, and automated-II methods, respectively. The

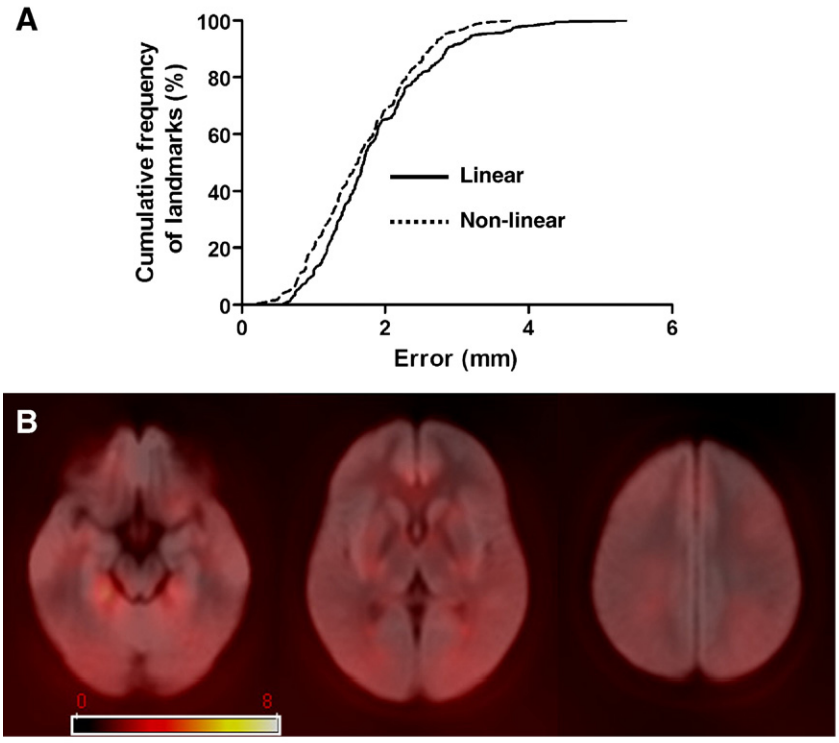


Fig. 4. Cumulative fraction of landmarks as a function of error.

higher coefficient of variation leads to lower statistical power when the method is used to detect abnormalities.

## Discussion

### *DTI-based atlases for white matter anatomy and brain normalization studies*

In the past, several DTI-based, single-subject white matter 3D atlases have been introduced (Catani et al., 2002; Hagmann et al., 2003; Makris et al., 1997; Mori et al., 2005; Pajevic and Pierpaoli, 1999; Stieltjes et al., 2001; Wakana et al., 2005). There are also excellent studies of probabilistic maps of specific white matter tracts (Burgel et al., 2006; Mori et al., 2002; Thottakara et al., 2006). In this paper, a population-averaged stereotaxic atlas of human white matter is introduced. In the past, most anatomical templates used for brain normalization studies did not have comprehensive information about white matter anatomy. In extreme cases, the white matter has been treated as a homogeneous entity with one compartment. DTI provides anatomical clues to identify structures and define their locations in the white matter. In the first step of this study, the population-averaged map in ICBM-152 coordinates (ICBM-DTI-81) was created using DTI data from 81 normal subjects and a 12-mode affine transformation. White matter structures that are appreciable in the ICBM-DTI-81 represent reproducible structures among normal adult subjects and their locations in the standardized coordinates. As can be seen in Fig. 2, all prominent white matter tracts can be clearly identified in this averaged map. In the second step, these structures were manually parcellated, based on their characteristic orientation information in the group-averaged map (WMPM).

For group analysis studies, the ICBM-DTI-81 provides various types of images (e.g., diffusion-weighted, non-diffusion-weighted [b0], FA, and tensor) (Fig. 2), which can be used as a template for brain normalization in the ICBM-152 coordinates. For example, if one wants to normalize FA maps, the population-averaged FA map of the ICBM-DTI-81 can be used as a target. The averaged tensor map (visualized as the color maps in Figs. 2E–H) could be used if, in the future, tensor-based brain transformation methods become available (Cao et al., 2005; Muller et al., 2007; Park et al., 2003; Zhang et al., 2006, 2005).

Table 1
Reproducibility measurement results for the manual and hybrid methods

| | $\kappa$ | | FA CoV (%) | |
|---|---|---|---|---|
| | Intra | Inter | Intra | Inter |
| Manual | 0.873±0.057 | 0.566±0.373 | 2.86±1.78 | 6.52±3.70 |
| Hybrid | 0.863±0.066 | 0.776±0.095 | 3.27±2.23 | 4.83±2.77 |

### *Creation of WMPM and usage*

Similar to cortical atlases, there is a certain degree of arbitrariness in the definition of the boundaries of the WMPM because many anatomical entities, such as the “corona radiata” and the “corpus callosum,” often do not have clear tissue boundaries. Therefore, the WMPM should be considered a guide for evaluating white matter anatomy rather than a gold standard for anatomical definition. There are several ways to use the WMPM. For example, if one is interested in studying white matter lesions, such as those occurring in multiple sclerosis or stroke patients, we often need to identify, report, and compare the lesion locations with those in other patients and correlate

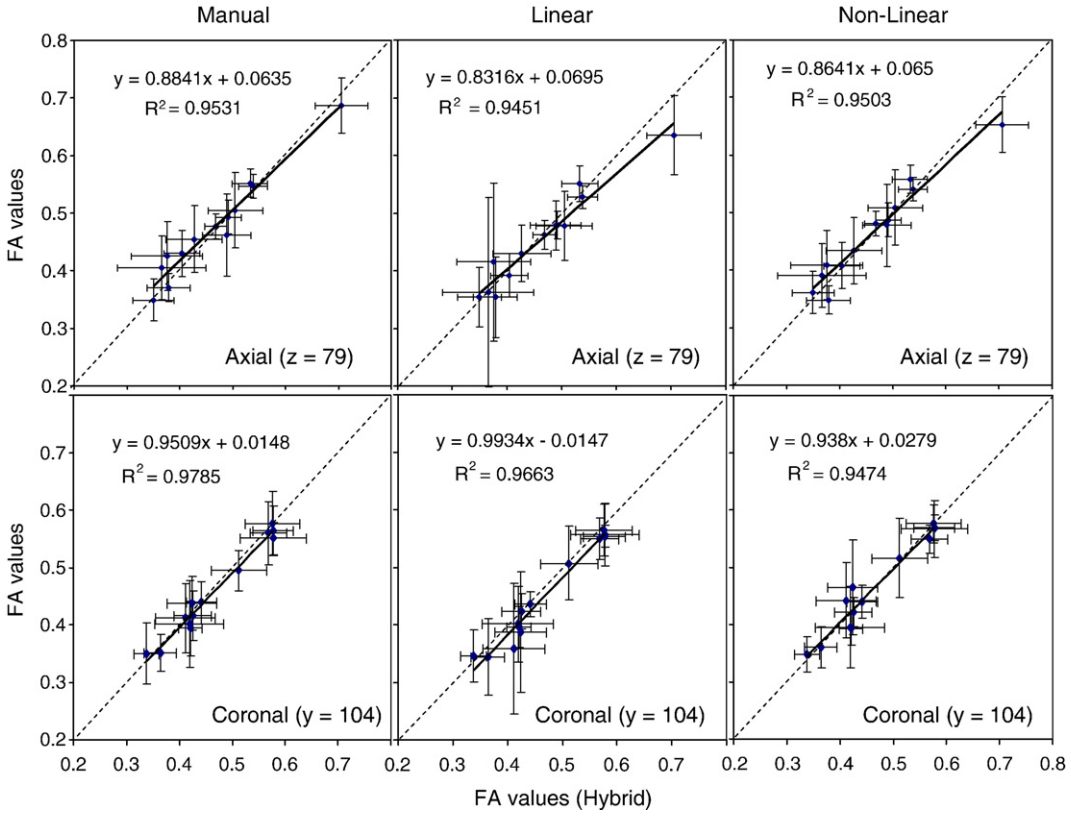


Fig. 5. Correlation plots between different quantification approaches described in Fig. 1. The hybrid method is used as a reference and compared to the other three approaches.

them with functional deficits (structure–function analyses). Template-based stereotaxic coordinates after brain normalization are widely used for these purposes. In this conventional approach, lesion locations are expressed as 3D standardized coordinates, in which each anatomical coordinate is treated as an independent entity. The WMPM can add another anatomical dimension by grouping voxels that belong to specific white matter structures; for example, two lesions in two patients with different normalized coordinates may belong to the same white matter tract. This new anatomical dimension added by the WMPM may increase the sensitivity and specificity of group analyses, such as identification of white matter tracts that are most sensitive to disease or involved in specific functional deficits.

*WMPM-based quantification and registration quality*

In order to measure MR parameters, such as FA, ADC, T2, or magnetization transfer ratio (MTR), manual ROI definition is one of the most widely adopted approaches. Although this is a valid approach, it has several drawbacks. First, it is usually hypothesis-driven, in which target brain regions and control regions are pre-selected based on expectation. Comprehensive analyses of the entire brain using multiple 3D ROIs may be possible, but would be too time-consuming for practical use. Second, the reproducibility of the manual delineation is often a subject of criticism. The pre-parcellated WMPM provides us with a means to evaluate the large number of white matter structures automatically and reproducibly, which could be a useful tool for initial whole-brain screening to assess the status of the brain and bring our attention to sensitive brain regions for more refined investigation.

In this paper, the WMPM was used for measuring regional intensities (i.e., FA) in two different ways; it was used as a guide for manual ROI drawing (manual and hybrid methods) or automated parcellation (Automated I and II). The high inter-rater reproducibility of the manual and hybrid approaches ($\kappa > 0.85$ and CoV < 3%) suggests that it is an effective guide for ROI drawing. With the hybrid approach, inter-rater reproducibility is also high ($\kappa > 0.75$ and CoV < 3%), which is attributable to the elimination of variability in slice selections among raters. The advantages of the hybrid approach include: (1) it can correct differences in brain orientations and, thus, extracted slices are likely to be more consistent across subjects; (2) objective criteria (i.e., the coordinates) for slice identification makes the ROI drawing process easier; and (3) the slice and ROI locations can be reported using a widely used coordinate system, such as ICBM-152.

In this study, we did not include the results of a manual ROI approach without using the WMPM as guidance. Usually, we need to determine some type of pre-defined (often visual) protocols to define ROIs. Without such protocols, the reproducibility of the definition of the border for some white matter tracts becomes very poor; for example, the corpus callosum in an axial or a coronal slice is often a continuous entity and different operators may use different anatomical clues to define the border. The WMPM can be considered one of the pre-defined, 3D, ROI drawing protocols in this regard. Our software, Landmarker and RoiEditor, provides interfaces for the brain normalization and the WMPM-guided ROI drawing.

Using the hybrid method as a reference, the accuracy of the automated methods was evaluated (Fig. 5). Although one of the advantages of the automated methods is 3D WMPM analysis, the comparison was limited to a representative 2D axial slice ($z = 79$ or

$y=104$) because it would be too time-consuming to manually define multiple (26 regions in this paper) 3D ROIs. Both the linear (Automated I) and non-linear (Automated II) methods show high correlation ($r^2>0.94$) for the FA values of the 26 anatomical regions. The Automated I method, however, has a large standard deviation among the normal population for several white matter tracts. The tracts with the highest variability are the right and left cingulum, which are small tracts, and a slight mis-registration can lead to significant inaccuracy.

While the rapid and 3D quantification by WMPM is a significant advantage over manual-based analyses, the drawback is that the accuracy depends on the quality of image normalization, which is often known to be inaccurate; if registration is poor, the WMPM would not align to the white matter structures of the subject. To measure the quality of structural alignment, we used landmark distances between the template and normalized subject data. The ICBM-DTI-81, which is based on normal population averages, provides registration errors mostly less than 3 mm. This registration quality may sound unexpectedly high, compared to previous reports based on cortical registration (Salmond et al., 2002; Thompson and Toga, 1996; Van Essen and Drury, 1997). However, this result is in line with previous registration studies measuring deep brain structures (Ardekani et al., 2005; Grachev et al., 1999).

We would like to emphasize that the registration quality measurements in this study are based on normal adult subjects and do not represent patients with significantly altered neuroanatomy. Compromised neuroanatomy in patients, such as enlarged ventricles, often cannot be normalized by linear transformation. In this case, the registration quality of the WMPM is expected to deteriorate. It is, therefore, very important to carefully interpret the results of automated MR intensity measurements. If abnormalities, such as reduced FA, are found in certain white matter regions, this could be due to anatomical changes and subsequent poorer registration in such areas. Visual inspection of registration quality and reexamination by manual ROI of such abnormal regions are recommended. If poor registration is the reason for the abnormal intensity values (e.g., decreased FA), it implies consistent anatomical differences, but not FA differences, in the abnormal area. In this case, size measurements of the putative structure may be advisable.

In this study, fourth-order polynomial transformation was used for non-linear transformation, which improved variability among the normal population observed with the linear normalization. However, the fourth-order transformation may not be elastic enough to remove large anatomical differences often observed in patient groups. To ensure better registration qualities, non-linear transformation with higher elasticity will be an important future effort. To fully exploit the advantages of high-order non-linear transformation, however, the population-averaged template may need to be recreated, because the ICBM-152 and ICBM-DTI-81, being obtained by linear normalization, do not have clear anatomical definition as a target of such transformation methods.

One important question that remains unanswered in this paper is the effect of age. In this paper, we pooled data from subjects from 18 to 59 years of age, assuming that the white matter anatomy is not significantly different among these age groups. If this assumption does not hold true, the precision of the atlas could be increased by creating multiple atlases at each age range. Similarly, it remains an important question whether our atlas can be applied to subjects older than 60 or younger than 18 years of age. These issues are also related to the accuracy of the normalization procedure; if the aged-dependent differences can be removed by the transformation method of choice, the impact of age would be minor. We need further studies to scrutinize the effects of age on the white matter anatomy and its relationship with transformation methods. Another important source of errors could be differences in imaging parameters, especially B0-susceptibility distortion. For example, images from 3-T scanners are often more distorted than those from 1.5-T scanners. After linear normalization, imperfect template–subject matching due to non-linear differences caused by individual anatomical differences, age-dependent differences, and image parameter-dependent differences remain as error sources, which leads to the imperfect correlation between the manual and automated approaches, as shown in Fig. 5. Our future efforts will focus on reducing these error sources by using higher-order, non-linear transformation, an age-matched template (if necessary), and imaging methods with less distortion.

## Conclusions

In conclusion, we have developed stereotaxic white matter atlases in the ICBM-152 (ICBM-DTI-81) coordinates and the software to utilize the atlas. This atlas can be used to associate white matter lesions to specific white matter structures using stereotaxic coordinates. After normalization of individual MRI images, MR parameters for pre-defined white matter regions are automatically measured by superimposing the WMPM. The registration quality measurements yield excellent results for the normal adult population, but for patients with anatomical alterations, future development of non-linear transformation may be needed. The atlas and associated software are downloadable from http://www.mristudio.org.

## Acknowledgments

This research was supported by NIH grants NCRR P41RR15241, U24RR021382, PO1 EB00195 and RO1AG20012. The National Center for Research Resources (NCRR) is a component of the National Institute of Health (NIH). The contents of this paper are solely the responsibility of the authors and do not necessarily represent the official view of NCRR or NIH. We would like to thank Dr. Alai Zhan for helping us to measure inter-rater reproducibility. Dr. Peter C.M. van Zijl is a paid lecturer for Philips Medical Systems. This arrangement has been approved by Johns Hopkins University in accordance with its conflict of interest policies.

## Appendix A

MNI coordinates of the landmarks used for measurements of normalization quality

| # | $x$[a] | $y$ | $z$ |
|---|---|---|---|
| Axial | | | |
| 1 | 24[b] | −32 | −16 |
| 2 | −26 | −32 | −16 |
| 3 | 34 | −8 | −16 |
| 4 | −36 | −8 | −16 |
| 5 | −24 | −36 | −11 |
| 6 | 22 | −36 | −11 |
| 7 | −34 | −18 | −11 |
| 8 | 32 | −18 | −11 |
| 9 | −34 | −5 | −11 |
| 10 | 32 | −5 | −11 |
| 11 | −17 | 35 | −11 |
| 12 | 15 | 35 | −11 |

**Appendix A** (*continued*)

| # | x[a] | y | z |
|---|---|---|---|
| Axial | | | |
| 13 | −21 | 15 | −11 |
| 14 | 19 | 15 | −11 |
| 15 | −39 | −33 | −11 |
| 16 | 37 | −33 | −11 |
| 17 | −22 | −43 | −5 |
| 18 | 20 | −43 | −5 |
| 19 | −30 | −32 | −5 |
| 20 | 28 | −32 | −5 |
| 21 | −23 | −25 | −5 |
| 22 | 21 | −25 | −5 |
| 23 | −6 | −5 | −5 |
| 24 | 4 | −5 | −5 |
| 25 | −42 | −22 | −5 |
| 26 | 40 | −22 | −5 |
| 27 | −12 | 37 | −5 |
| 28 | 11 | 37 | −5 |
| 29 | −17 | 16 | −5 |
| 30 | 16 | 16 | −5 |
| 31 | −27 | 0 | −5 |
| 32 | 25 | 0 | −5 |
| 33 | −40 | −34 | −5 |
| 34 | 38 | −34 | −5 |
| 35 | −37 | −52 | −5 |
| 36 | 35 | −52 | −5 |
| 37 | −31 | −68 | −5 |
| 38 | 29 | −68 | −5 |
| 39 | −21 | −48 | 0 |
| 40 | 19 | −48 | 0 |
| 41 | −29 | −35 | 0 |
| 42 | 27 | −35 | 0 |
| 43 | −31 | −24 | 0 |
| 44 | 29 | −24 | 0 |
| 45 | −10 | −2 | 0 |
| 46 | 8 | −2 | 0 |
| 47 | −31 | −2 | 0 |
| 48 | 29 | −2 | 0 |
| 49 | −21 | 15 | 0 |
| 50 | 20 | 15 | 0 |
| 51 | −7 | 27 | 0 |
| 52 | 6 | 27 | 0 |
| 53 | −17 | 27 | 0 |
| 54 | 16 | 27 | 0 |
| 55 | −38 | −47 | 0 |
| 56 | 36 | −47 | 0 |
| 57 | −33 | −63 | 0 |
| 58 | 31 | −63 | 0 |
| 59 | −26 | −76 | 0 |
| 60 | 24 | −76 | 0 |
| 61 | −13 | −52 | 8 |
| 62 | 11 | −52 | 8 |
| 63 | −27 | −41 | 8 |
| 64 | 24 | −41 | 8 |
| 65 | −30 | −26 | 8 |
| 66 | 28 | −26 | 8 |
| 67 | −9 | −5 | 8 |
| 68 | 7 | −5 | 8 |
| 69 | −31 | −5 | 8 |
| 70 | 29 | −5 | 8 |
| 71 | −24 | 13 | 8 |
| 72 | 22 | 13 | 8 |
| 73 | −8 | 33 | 8 |
| 74 | 6 | 33 | 8 |
| 75 | −19 | 27 | 8 |
| 76 | 17 | 27 | 8 |
| 77 | −35 | −48 | 8 |
| 78 | 32 | −48 | 8 |
| 79 | −31 | −65 | 8 |
| 80 | 29 | −65 | 8 |
| 81 | −24 | −79 | 8 |
| 82 | 22 | −79 | 8 |
| 83 | −12 | −55 | 14 |
| 84 | 9 | −55 | 14 |
| 85 | −24 | −40 | 14 |
| 86 | 22 | −40 | 14 |
| 87 | −29 | −24 | 14 |
| 88 | 27 | −24 | 14 |
| 89 | −11 | −3 | 14 |
| 90 | 10 | −3 | 14 |
| 91 | −29 | −3 | 14 |
| 92 | 27 | −3 | 14 |
| 93 | −25 | 9 | 14 |
| 94 | 23 | 9 | 14 |
| 95 | −8 | 32 | 14 |
| 96 | 6 | 32 | 14 |
| 97 | −19 | 25 | 14 |
| 98 | 18 | 25 | 14 |
| 99 | −37 | −46 | 14 |
| 100 | 35 | −46 | 14 |
| 101 | −30 | −62 | 14 |
| 102 | 28 | −62 | 14 |
| 103 | −22 | −76 | 14 |
| 104 | 20 | −76 | 14 |
| 105 | −10 | −55 | 20 |
| 106 | 8 | −55 | 20 |
| 107 | −26 | −50 | 20 |
| 108 | 24 | −50 | 20 |
| 109 | −8 | 27 | 20 |
| 110 | 6 | 27 | 20 |
| 111 | −19 | 21 | 20 |
| 112 | 18 | 20 | 20 |
| 113 | −27 | 11 | 20 |
| 114 | 25 | 11 | 20 |
| 115 | −15 | −7 | 20 |
| 116 | 14 | −7 | 20 |
| 117 | −30 | −36 | 20 |
| 118 | 28 | −36 | 20 |
| 119 | −35 | −47 | 20 |
| 120 | 33 | −47 | 20 |
| 121 | −26 | −67 | 20 |
| 122 | 24 | −67 | 20 |
| 123 | −10 | −52 | 27 |
| 124 | 9 | −52 | 27 |
| 125 | −8 | 17 | 27 |
| 126 | 6 | 17 | 27 |
| 127 | −27 | 20 | 27 |
| 128 | 25 | 20 | 27 |
| 129 | −29 | 1 | 27 |
| 130 | 28 | 1 | 27 |
| 131 | −32 | −19 | 27 |
| 132 | 31 | −19 | 27 |
| 133 | −32 | −47 | 27 |
| 134 | 29 | −47 | 27 |
| 135 | −23 | 18 | 33 |

*(continued on next page)*

**Appendix A** (*continued*)

| # | x[a] | y | z |
|---|---|---|---|
| Axial | | | |
| 136 | 22 | 18 | 33 |
| 137 | −30 | 0 | 33 |
| 138 | 28 | 0 | 33 |
| 139 | −32 | −26 | 33 |
| 140 | 30 | −26 | 33 |
| 141 | −28 | −51 | 33 |
| 142 | 26 | −51 | 33 |
| 143 | −20 | 19 | 39 |
| 144 | 19 | 19 | 39 |
| 145 | −23 | 2 | 39 |
| 146 | 23 | 2 | 39 |
| 147 | −28 | −24 | 39 |
| 148 | 27 | −24 | 39 |
| 149 | −25 | −46 | 39 |
| 150 | 24 | −46 | 39 |
| 151 | −18 | 16 | 46 |
| 152 | 17 | 16 | 46 |
| 153 | −21 | −7 | 46 |
| 154 | 20 | −7 | 46 |
| 155 | −24 | −30 | 46 |
| 156 | 22 | −30 | 46 |
| 157 | −24 | −53 | 46 |
| 158 | 22 | −53 | 46 |
| Sagittal | | | |
| 1 | 0 | 0 | 0 |
| 2 | 0 | −34 | 0 |
| 3 | 0 | −34 | −16 |
| 4 | 0 | −27 | −17 |
| 5 | 0 | −38 | −40 |
| 6 | 0 | −32 | −45 |
| 7 | 0 | 22 | 2 |
| 8 | 0 | 29 | 9 |
| 9 | 0 | 17 | 9 |
| 10 | 0 | −44 | 7 |
| 11 | 0 | −37 | 16 |
| 12 | 0 | −49 | 16 |
| 13 | 0 | 0 | 24 |
| 14 | 0 | −34 | 20 |
| 15 | 0 | −20 | −21 |
| Coronal | | | |
| 1 | −8 | 12 | 30 |
| 2 | 6 | 12 | 30 |
| 3 | −24 | 12 | 35 |
| 4 | 23 | 12 | 35 |
| 5 | −22 | 12 | 26 |
| 6 | 21 | 12 | 26 |
| 7 | −14 | 12 | −4 |
| 8 | 13 | 12 | −4 |
| 9 | −8 | −2 | 36 |
| 10 | 6 | −2 | 36 |
| 11 | −28 | −2 | 35 |
| 12 | 27 | −2 | 35 |
| 13 | −20 | −2 | 30 |
| 14 | 19 | −2 | 30 |
| 15 | −29 | −2 | 19 |
| 16 | 27 | −2 | 19 |
| 17 | −33 | −2 | 4 |
| 18 | 31 | −2 | 4 |
| 19 | −11 | −2 | 1 |
| 20 | 9 | −2 | 1 |
| 21 | −33 | −2 | −6 |
| 22 | 31 | −2 | −6 |

**Appendix A** (*continued*)

| # | x[a] | y | z |
|---|---|---|---|
| Coronal | | | |
| 23 | −8 | −15 | 38 |
| 24 | 6 | −15 | 38 |
| 25 | −30 | −15 | 38 |
| 26 | 28 | −15 | 38 |
| 27 | −21 | −15 | 32 |
| 28 | 20 | −15 | 32 |
| 29 | −31 | −15 | 27 |
| 30 | 30 | −15 | 28 |
| 31 | −36 | −15 | 5 |
| 32 | 34 | −15 | 5 |
| 33 | −33 | −15 | −11 |
| 34 | 31 | −15 | −11 |
| 35 | −44 | −15 | −19 |
| 36 | 42 | −15 | −19 |
| 37 | −24 | −15 | −27 |
| 38 | 22 | −15 | −26 |
| 39 | −9 | −29 | 36 |
| 40 | 7 | −29 | 36 |
| 41 | −27 | −29 | 45 |
| 42 | 26 | −29 | 45 |
| 43 | −32 | −29 | 37 |
| 44 | 30 | −29 | 37 |
| 45 | −32 | −29 | 26 |
| 46 | 31 | −29 | 26 |
| 47 | −32 | −29 | 9 |
| 48 | 30 | −29 | 9 |
| 49 | −40 | −29 | −10 |
| 50 | 38 | −29 | −10 |
| 51 | −30 | −29 | −5 |
| 52 | 28 | −29 | −5 |
| 53 | −26 | −29 | −18 |
| 54 | 24 | −29 | −18 |
| 55 | −27 | −46 | 36 |
| 56 | 25 | −46 | 36 |
| 57 | −35 | −46 | 20 |
| 58 | 33 | −46 | 20 |
| 59 | −41 | −46 | 6 |
| 60 | 39 | −46 | 6 |
| 61 | −25 | −61 | 15 |
| 62 | 23 | −61 | 15 |
| 63 | −34 | −61 | 1 |
| 64 | 32 | −61 | 1 |

[a] *x*, *y*, and *z* represent right–left, anterior–posterior, and superior–inferior axes, respectively.

[b] Coordinates in millimeters with respect to the anterior commissure at the mid-sagittal slice.

## References

Alexander, D.C., Pierpaoli, C., Basser, P.J., Gee, J.C., 2001. Spatial transformations of diffusion tensor magnetic resonance images. IEEE Trans. Med. Imaging 20, 1131–1139.

Ardekani, B.A., Guckemus, S., Bachman, A., Hoptman, M.J., Wojtaszek, M., Nierenberg, J., 2005. Quantitative comparison of algorithms for inter-subject registration of 3D volumetric brain MRI scans. J. Neurosci. Methods 142, 67–76.

Basser, P.J., Mattiello, J., Le Bihan, D., 1994a. MR diffusion tensor spectroscopy and imaging. Biophys. J. 66, 259–267.

Basser, P.J., Mattiello, J., LeBihan, D., 1994b. Estimation of the effective self-diffusion tensor from the NMR spin echo. J. Magn. Reson. B 103, 247–254.

Basser, P.J., Pajevic, S., Pierpaoli, C., Duda, J., Aldroubi, A., 2000. In vitro fiber tractography using DT-MRI data. Magn. Reson. Med. 44, 625–632.

Brodmann, K., 1909. Vergleichende lokalisationlehre der grosshirnrinde in ihren prinziprien dargestellt auf grund des zellenbaues. Leipzig, Barth.

Burgel, U., Amunts, K., Hoemke, L., Mohlberg, H., Gilsbach, J.M., Zilles, K., 2006. White matter fiber tracts of the human brain: three-dimensional mapping at microscopic resolution, topography and intersubject variability. Neuroimage 29, 1092–1105.

Cao, Y., Miller, M.I., Winslow, R.L., Younes, L., 2005. Large deformation diffeomorphic metric mapping of vector fields. IEEE Trans. Med. Imaging 24, 1216–1230.

Carpenter, M., 1976. Human Neuroanatomy. Williams & Wilkins, Baltimore.

Catani, M., Howard, R.J., Pajevic, S., Jones, D.K., 2002. Virtual in vivo interactive dissection of white matter fasciculi in the human brain. Neuroimage 17, 77–94.

Collins, D.L., Neelin, P., Peters, T.M., Evans, A.C., 1994. Automatic 3D intersubject registration of MR volumetric data in standardized Talairach space. J. Comput. Assist. Tomogr. 18, 192–205.

Conturo, T.E., Lori, N.F., Cull, T.S., Akbudak, E., Snyder, A.Z., Shimony, J.S., McKinstry, R.C., Burton, H., Raichle, M.E., 1999. Tracking neuronal fiber pathways in the living human brain. Proc. Natl. Acad. Sci. U. S. A. 96, 10422–10427.

Crosby, E., Humphrey, T., Lauer, E., 1962. Correlative Anatomy of the Nervous System. MacMillan, New York.

Douek, P., Turner, R., Pekar, J., Patronas, N., Le Bihan, D., 1991. MR color mapping of myelin fiber orientation. J. Comput. Assist.Tomogr. 15, 923–929.

Evans, A., Collins, D.L., Milner, B., 1992. An MRI-based stereotactic atlas from 250 young normal subjects. J. Soc. Neurosci. Abstr. 18, 408.

Grachev, I.D., Berdichevsky, D., Rauch, S.L., Heckers, S., Kennedy, D.N., Caviness, V.S., Alpert, N.M., 1999. A method for assessing the accuracy of intersubject registration of the human brain using anatomic landmarks. Neuroimage 9, 250–268.

Hagmann, P., Thiran, J.P., Jonasson, L., Vandergheynst, P., Clarke, S., Maeder, P., Meuli, R., 2003. DTI mapping of human brain connectivity: statistical fibre tracking and virtual dissection. Neuroimage 19, 545–554.

Jellison, B.J., Field, A.S., Medow, J., Lazar, M., Salamat, M.S., Alexander, A.L., 2004. Diffusion tensor imaging of cerebral white matter: a pictorial review of physics, fiber tract anatomy, and tumor imaging patterns. AJNR Am. J. Neuroradiol. 25, 356–369.

Jiang, H., van Zijl, P.C., Kim, J., Pearlson, G.D., Mori, S., 2006. DtiStudio: resource program for diffusion tensor computation and fiber bundle tracking. Comput. Methods Programs Biomed. 81, 106–116.

Jones, D.K., Horsfield, M.A., Simmons, A., 1999. Optimal strategies for measuring diffusion in anisotropic systems by magnetic resonance imaging. Magn. Reson. Med. 42, 515–525.

Lancaster, J.L., Woldorff, M.G., Parsons, L.M., Liotti, M., Freitas, C.S., Rainey, L., Kochunov, P.V., Nickerson, D., Mikiten, S.A., Fox, P.T., 2000. Automated Talairach atlas labels for functional brain mapping. Hum. Brain Mapp. 10, 120–131.

Makris, N., Worth, A.J., Sorensen, A.G., Papadimitriou, G.M., Reese, T.G., Wedeen, V.J., Davis, T.L., Stakes, J.W., Caviness, V.S., Kaplan, E., Rosen, B.R., Pandya, D.N., Kennedy, D.N., 1997. Morphometry of in vivo human white matter association pathways with diffusion weighted magnetic resonance imaging. Ann. Neurol. 42, 951–962.

Makris, N., Kennedy, D.N., McInerney, S., Sorensen, A.G., Wang, R., Caviness Jr., V.S., Pandya, D.N., 2005. Segmentation of subcomponents within the superior longitudinal fascicle in humans: a quantitative, in vivo, DT-MRI study. Cereb. Cortex 15, 854–869.

Mazziotta, J.C., Toga, A.W., Evans, A., Fox, P., Lancaster, J., 1995. A probabilistic atlas of the human brain: theory and rationale for its development. The International Consortium for Brain. Mapping (ICBM). Neuroimage 2, 89–101.

Mori, S., Crain, B.J., Chacko, V.P., van Zijl, P.C.M., 1999. Three dimensional tracking of axonal projections in the brain by magnetic resonance imaging. Ann. Neurol. 45, 265–269.

Mori, S., Kaufmann, W.E., Davatzikos, C., Stieltjes, B., Amodei, L., Fredericksen, K., Pearlson, G.D., Melhem, E.R., Solaiyappan, M., Raymond, G.V., Moser, H.W., van Zijl, P.C.M., 2002. Imaging cortical association tracts in human brain. Magn. Reson. Med. 47, 215–223.

Mori, S., Wakana, S., Nagae-Poetscher, L.M., van Zijl, P.C., 2005. MRI Atlas of Human White Matter. Elsevier, Amsterdam, The Netherlands.

Muller, H.P., Unrath, A., Ludolph, A.C., Kassubek, J., 2007. Preservation of diffusion tensor properties during spatial normalization by use of tensor imaging and fibre tracking on a normal brain database. Phys. Med. Biol. 52, N99–N109.

Nakada, T., Matsuzawa, H., 1995. Three-dimensional anisotropy contrast magnetic resonance imaging of the rat nervous system: MR axonography. Neurosc. Res. 22, 389–398.

Nieuwenhuys, R., Voogd, J., van Huijzen, C., 1983. The Human Central Nervous System. Springer-Verlag.

Pajevic, S., Pierpaoli, C., 1999. Color schemes to represent the orientation of anisotropic tissues from diffusion tensor data: application to white matter fiber tract mapping in the human brain. Magn. Reson. Med. 42, 526–540.

Park, H.J., Kubicki, M., Shenton, M.E., Guimond, A., McCarley, R.W., Maier, S.E., Kikinis, R., Jolesz, F.A., Westin, C.F., 2003. Spatial normalization of diffusion tensor MRI using multiple channels. Neuroimage 20, 1995–2009.

Parker, G.J., Stephan, K.E., Barker, G.J., Rowe, J.B., MacManus, D.G., Wheeler-Kingshott, C.A., Ciccarelli, O., Passingham, R.E., Spinks, R.L., Lemon, R.N., Turner, R., 2002. Initial demonstration of in vivo tracing of axonal projections in the macaque brain and comparison with the human brain using diffusion tensor imaging and fast marching tractography. Neuroimage 15, 797–809.

Pierpaoli, C., Basser, P.J., 1996. Toward a quantitative assessment of diffusion anisotropy. Magn. Reson. Med. 36, 893–906.

Pierpaoli, C., Jezzard, P., Basser, P.J., Barnett, A., Di Chiro, G., 1996. Diffusion tensor MR imaging of human brain. Radiology 201, 637–648.

Poupon, C., Clark, C.A., Frouin, V., Regis, J., Bloch, L., Le Bihan, D., Mangin, J.F., 2000. Regularization of diffusion-based direction maps for the tracking of brain white matter fascicules. Neuroimage 12, 184–195.

Pruessmann, K.P., Weiger, M., Scheidegger, M.B., Boesiger, P., 1999. SENSE: sensitivity encoding for fast MRI. Magn. Reson. Med. 42, 952–962.

Salmond, C.H., Ashburner, J., Vargha-Khadem, F., Connelly, A., Gadian, D.G., Friston, K.J., 2002. The precision of anatomical normalization in the medial temporal lobe using spatial basis functions. Neuroimage 17, 507–512.

Stieltjes, B., Kaufmann, W.E., van Zijl, P.C.M., Fredericksen, K., Pearlson, G.D., Mori, S., 2001. Diffusion tensor imaging and axonal tracking in the human brainstem. Neuroimage 14, 723–735.

Talairach, J., Tournoux, P., 1988. Co-Planar Stereotaxic Atlas of the Human Brain. 3-Dimensional Proportional System: An Approach to Cerebral Imaging. Thieme Medical, New York, NY.

Thompson, P.M., Toga, A.W., 1996. A surface-based technique for warping three-dimensional images of the brain. IEEE Trans. Med. Imaging 15, 402–417.

Thottakara, P., Lazar, M., Johnson, S.C., Alexander, A.L., 2006. Application of Brodmann's area templates for ROI selection in white matter tractography studies. Neuroimage 29, 868–878.

Toga, A.W., Thompson, P.M., Mori, S., Amunts, K., Zilles, K., 2006. Towards multimodal atlases of the human brain. Nat. Rev. Neurosci. 7, 952–966.

Ture, U., Yasargil, M., Pait, T., 1997. Is there a superior occipitofrontal fasciculus? A microsurgical anatomic study. Neurosurgery 40, 1226–1232.

Van Essen, D.C., Drury, H.A., 1997. Structural and functional analyses of human cerebral cortex using a surface-based atlas. J. Neurosci. 17, 7079–7102.

Wakana, S., Jiang, H., Nagae-Poetscher, L.M., Van Zijl, P.C., Mori, S., 2004. Fiber tract-based atlas of human white matter anatomy. Radiology 230, 77–87.

Wakana, S., Nagae-Poetscher, L.M., Jiang, H., van Zijl, P., Golay, X., Mori, S., 2005. Macroscopic orientation component analysis of brain white

matter and thalamus based on diffusion tensor imaging. Magn. Reson. Med. 53, 649–657.

Woods, R.P., Grafton, S.T., Holmes, C.J., Cherry, S.R., Mazziotta, J.C., 1998. Automated image registration: I. General methods and intrasubject, intramodality validation. J. Comput. Assist. Tomogr. 22, 139–152.

Xu, D., Mori, S., Shen, D., van Zijl, P.C., Davatzikos, C., 2003. Spatial normalization of diffusion tensor fields. Magn. Reson. Med. 50, 175–182.

Zhang, H., Yushkevich, P.A., Gee, J.C., 2005. Deformable registration of diffusion tensor MR images with explicit orientation optimization. Med. Image Comput. Comput. Assist. Interv. Int. Conf. Med. Image Comput. Comput. Assist. Interv. 8, 172–179.

Zhang, H., Yushkevich, P.A., Alexander, D.C., Gee, J.C., 2006. Deformable registration of diffusion tensor MR images with explicit orientation optimization. Med. Image Anal. 10, 764–785.